JGR Space Physics

RESEARCH ARTICLE
10.1029/2022JA031166

A Comparative Study on the Hot Dense Plasma and Cold Patch by Using Multi-Instrument Observations

Yu-Zhang Ma[1], Qing-He Zhang[1], Larry Lyons[2], Kjellmar Oksavik[3,4], Zan-Yang Xing[1], Marc Hairston[5], Balan Nanan[1], Ze-Jun Hu[6], Yong Wang[1], and Si-Han Zhao[1]

[1]Shandong Provincial Key Laboratory of Optical Astronomy and Solar-Terrestrial Environment, Institute of Space Sciences, Shandong University, Weihai, China, [2]Department of Atmospheric and Oceanic Sciences, University of California, Los Angeles, CA, USA, [3]Birkeland Centre for Space Science, University of Bergen, Bergen, Norway, [4]Arctic Geophysics, University Centre in Svalbard, Longyearbyen, Norway, [5]William B. Hanson Center for Space Sciences, University of Texas at Dallas, Richardson, TX, USA, [6]MNR Key Laboratory for Polar Science, Polar Research Institute of China, Shanghai, China

Abstract The polar cap hot patch is an enhanced density structure which is associated with particle precipitation, ion upflow and flow shears. Based on combined observations from DMSP satellites, EISCAT radar, and all-sky imager at the Chinese Yellow River Station, the plasma characteristics and evolution of hot dense plasma and classical polar cap patch are investigated. Both of them show enhanced F region density, but the hot dense plasma is associated with higher electron temperature and enhanced E region electron density caused by particle precipitation. Compared to the cold patch, the hot dense plasma is closer to the cusp region and is associated with strong auroral emissions. Based on the joint observations, the evolution of the hot/cold dense plasma is discussed. In the initial phase the dense plasma comes from the sunlit lower latitude region, or from particle precipitation in the duskside auroral oval, and is heated locally by poleward moving auroral structures in the dayside auroral oval. Next the patches move poleward into the polar cap where a decaying electron temperature (i.e., less precipitation) gradually transform them into a cold patch.

Plain Language Summary The polar cap hot patch is a high-density ionospheric irregularity with enhanced electron temperature and particle precipitation. The density source and associated auroral emission of the hot patch are not clear. The relationship between the hot dense plasma (hot patch) and classical polar cap patch (cold patch) is a lingering question. In this paper, we show two hot dense plasma and cold patch events using multi-instrument observations. Two density sources are suggested: dense plasma in the lower latitude sunlit region, and plasma ionized by particle precipitation in the duskside auroral oval. Our study shows the hot dense plasma is associated with stronger aurora emissions and higher E region density in the cusp region, followed by no auroral emission (colder electron temperature) as the hot dense plasma drifts poleward and turns into a cold patch in the polar cap. It suggests that the hot dense plasma and cold patch may be different states of the same irregularity structure.

Key Points:

- The different plasma characteristics of hot dense plasma and cold patch in the polar cap are investigated using multi-instrument observations
- Both hot dense plasma and cold patches are associated with auroral forms, which are located further equatorward in the cusp region
- The hot dense plasma and cold patch may represent different energy states of the same plasma structure as it traverses the polar ionosphere

Supporting Information:

Supporting Information may be found in the online version of this article.

Correspondence to:

Q.-H. Zhang,
zhangqinghe@sdu.edu.cn

Citation:

Ma, Y.-Z., Zhang, Q.-H., Lyons, L., Oksavik, K., Xing, Z.-Y., Hairston, M., et al. (2023). A comparative study on the hot dense plasma and cold patch by using multi-instrument observations. *Journal of Geophysical Research: Space Physics*, *128*, e2022JA031166. https://doi.org/10.1029/2022JA031166

Received 17 NOV 2022
Accepted 18 MAY 2023

Author Contributions:

Software: Yong Wang

1. Introduction

Polar cap patches are defined as high density ionospheric islands having densities at least two times that of the surrounding background polar cap ionospheric plasma (Crowley, 1996; Zhang et al., 2017). The typical spatial sizes of polar cap patches range from ~100 to 1,000 km (Carlson, 2012; Crowley, 1996; Moen, Qiu, et al., 2008; Zhang et al., 2021). The density profile inside a patch typically shows a strong increasement between 200 and 600 km altitude, and usually peaks in the F region around 300 km with densities of 10^5 cm^{-3} (Nishimura et al., 2021; Zhang et al., 2011). Ionization by solar extreme ultraviolet radiation at the mid-latitude region and particle precipitation in the cusp region are believed to be the source of the high electron density in polar cap patches (Goodwin et al., 2015; Lockwood et al., 2005; Moen, Qiu, et al., 2008; Oksavik et al., 2006; Zhang et al., 2013, 2015). The formation mechanisms are therefore suggested to be the following: Interplanetary magnetic field (IMF) modifies the cusp convection flow pattern and causes periods of both dense and of low-density plasma from lower latitudes to enter the cusp alternately (Milan et al., 2002); plasma depletion within flow-burst channels due to enhanced recombination, associated with the rapid motion of newly opened magnetic flux tubes (Pitout & Blelly, 2003; Rodger et al., 1994); transient periods of enhanced dayside reconnection that configures the open-closed field line boundary (OCB) to expand equatorward into the lower latitude sunlit region, drawing the EUV ionized plasma into the polar flow, which, when the OCB retreats poleward (Carlson et al., 2006; Lockwood et al., 2000;

Zhang et al., 2011, 2013). MacDougall and Jayachandran (2007) suggested that plasma transport from the auroral precipitation regions can also dominate polar cap patch production. In some cases, the patches can be generated by PMAFs associated with auroral particle precipitation (Lorentzen et al., 2010; Nishimura et al., 2014).

The type/class of polar cap patches is usually identified/classified by their plasma characteristics using in-situ observations from satellites or ground-based radars. With the European incoherent scatter radar (EISCAT) two types of patches (type L and H) are found in the cusp region with different electron temperature and electron density (Zhang et al., 2013). DMSP satellite observed a type of "hot patch" which is similar to type H (Zhang et al., 2017). The hot patch is associated with strong particle precipitation, enhanced electron temperature and field-aligned currents right near the dayside auroral oval. Particle precipitation is expected to be its density source (Zhang et al., 2017). However, if type H patch is hot patch should be confirmed. The statistical results reported by Zhang et al. (2022) show that the hot patch occurrence is not only associated with the precipitated electron energy flux, but also associated with strong anti-sunward flow velocity. Thus, the density source of the hot patch still needs to be studied, and the relationship between the hot and cold patches remain unclear.

In this paper, we combine observations from in-situ DMSP F16 satellite and ground-based instruments to evaluate two types of polar cap patches seen on 8 December 2013 and 9 December 2015. The ground-based instruments include all-sky imagers at the Chinese Yellow River Station, the EISCAT Svalbard incoherent scatter radar, total electron content data from the Madrigal database, and SuperDARN High-Frequency (HF) radar observations. We will document the plasma characteristics of the two different types of patches as seen in the multi-instrument observations and use this information to infer the density source of the different patches and their physical relations.

2. Data Sources

2.1. DMSP

DMSP satellites operate in sun-synchronous polar orbits with ~100 min period at ~800 km altitude. Data from DMSP F16 are used in this study, including: (a) the density, temperature and velocity data at 4 s time resolution from the Special Senor for Ions, Electrons, and Scintillation (SSIES), (b) the differential energy flux of precipitated ions and electrons at 1 s time resolution from special sensor for precipitating particles (SSJ/4) in the energy ranges of 30 eV to 30 keV, and (c) the magnetic field data at 1 s time resolution from the spatial magnetic field detectors (SSM) (Hardy et al., 1984; Rich & Hairston, 1994).

2.2. All-Sky Imagers

The all-sky imagers are installed at the Chinese Yellow River Station (YRS-ASI) (78.92°N, 11.93°E in geographic coordinate) at Ny-Ålesund, Svalbard (Hu et al., 2009). These imagers offer optical observations at 427.8 nm, 557.7 nm, and 630.0 nm during winter months (November to February). In this paper we use 557.7 and 630.0 nm all-sky images at 10 s time resolution to illustrate the evolution of cusp region auroral emissions and polar cap patches.

2.3. EISCAT

The European Incoherent Scatter Radar (EISCAT) network offers ionospheric and atmospheric measurements north of the Arctic circle. Data from the 32 m steerable antenna and 42m field-aligned antenna of the EISCAT Svalbard Radar (ESR, 78.15°N 16.03°E in geographic coordinates) at Longyearbyen, Svalbard, is used in this paper, including electron density, electron and ion temperature, and line-of-sight ion velocity. These parameters are available at 1 min time resolution.

2.4. SuperDARN and GNSS-TEC

The Super Dual Auroral Radar Network (SuperDARN) consists of more than 30 low-power HF radars looking into Earth's upper atmosphere and ionosphere at mid, high, and polar latitudes, which offers continuous monitoring of the ionospheric plasma motion. The fitted 2-min convection data is used in this paper. The Madrigal database is a community resource for geospace data. Global Navigation Satellite Systems Total Electron Content

(GNSS-TEC) data is obtained from that database with 5-min resolution, and median filtering is applied in a 1° in latitude by 2° in longitude grid. We also use 1-min TEC data from four GNSS receivers operated by the University of Bergen (Oksavik, 2020a, 2020b, 2020a). The receiver geographic latitudes (GLAT), geographic longitudes (GLON), and magnetic latitudes (MLAT, Altitude Adjusted Corrected Geomagnetic Coordinates (AACGM) (Baker & Wing, 1989)) are Ny-Ålesund (78.9° GLAT, 11.9° GLON, 76.4° MLAT), Longyearbyen (78.1° GLAT, 16.0° GLON, 75.4° MLAT), Hopen (76.5° GLAT, 25.0° GLON, 73.3° MLAT), and Bjørnøya (74.5° GLAT, 19.0° GLON, 71.6° MLAT).

3. Observations

3.1. Event on 9 December 2015

On 9 December 2015, DMSP F16 crossed the polar region in the Northern Hemisphere at 11:49-12:14 universal time (UT). The IMF conditions and in-situ plasma observations are shown in Figure 1, and each panel from top to bottom is: IMF components with the time of the DMSP passage marked by black dashed lines, total ion and O^+ number density (Ni, No), temperature of electrons and ions (Te, Ti), horizontal (cross-track) and vertical velocity (V_{hor}, V_{ver}), field-aligned current (FAC, $J_{//}$), differential energy flux of electrons and ions. The IMF components come from the OMNI dataset and a 7 min delay is applied. The DMSP F16 transit is marked by black dashed lines. The horizontal velocity is positive pointing sunward. The field-aligned current is calculated by dividing magnetic disturbance with satellite velocity, the details are described in Ma et al. (2020). IMF Bz turns southward after 11:45 UT, and it is weak negative throughout the satellite transit. IMF Bx and By are steadily negative and positive, respectively. The solar wind density (~4.2 cm^{-3}) and solar wind velocity (450 km/s) do not change throughout this time (Figure S1). A dense plasma structure is marked by the red dashed lines at 11:58-12:00 UT. The ion density is about $0.5 - 1 \times 10^4 cm^{-3}$ and shows a sharp density gradient around its boundaries. Inside the dense plasma structure, the convection first points sunward and then turns to anti-sunward at 11:59:20 UT associated with soft electron (<10^3 eV) and ion (10^2~10^4 eV) precipitation, indicating it may be in the low latitude boundary layer (LLBL) (Newell et al., 1991; Sandholt et al., 2002). Thus, in the following part, we will divide this density structure into the "sunward moving part" and the "anti-sunward moving part" to describe the different plasma characteristics between the two parts.

In the sunward moving part, the averaged ion density is $\sim 0.6 \times 10^4 cm^{-3}$ and the electron temperature is around 1000 K higher than ion temperature; enhanced soft electron and <10 keV ion precipitation are observed at the same time. In the anti-sunward moving part of the hot dense plasma, the electron temperature decreases to the same level as the ion temperature after 11:59:30 UT, and both electron and ion precipitation reduce during this period. However, the ion density $\left(1 \times 10^4 cm^{-3}\right)$ is two times higher than within the sunward part until the satellite leaves the dense plasma structure at 12:00 UT. The field-aligned current is first downward, then upward at 11:59:00–11:59:30 UT, and the upward current peaks right at the flow reversal region between these two parts. Poleward of the dense plasma structure, convection becomes very weak before turning anti-sunward well within the polar cap. In general, based on these observational features, although the sunward moving portion of the dense structure is located within the auroral oval, the full structure shows similar plasma characteristics of the hot patch (Ma et al., 2018; Zhang et al., 2017, 2021).

To investigate the formation and evolution of this hot, dense plasma (or hot patch for its dense and hot characteristics), Figure 2 is given to show the sequences of multi-instrument observations. The YRS-ASI 630.0 nm (red band) auroral emission and DMSP observations are given in the left panels, and the GPS-TEC map overlaid by SuperDARN convection patterns are presented in the right panels. The ESR 42m antenna points along the magnetic field line as indicated by a black triangle in the plots. The DMSP F16 or F18 orbit is shown in all panels, where the colored dots and the magenta lines indicate the O^+ number density in log scale and the horizontal velocity, respectively. Along the satellite trajectory, the location of the hot dense plasma on F16 and F18 is marked by the black solid lines in panels b1 (it is not there anymore) and c1, respectively. Animations of the red and green band emissions are given in supplementary movies S1 and S2 at 10 s cadence, respectively. The TEC movie is given in Movie S3 at 5 min cadence.

Figure 2a1 shows the auroral oval crossed the middle of the YRS-ASI field-of-view (FOV), and an area of brightened aurora observed in the western part of the FOV. At 11:45 UT, DMSP F18 crossed this area and observed a westward flow with enhanced O^+ density, enhanced electron temperature and particle precipitation (Figure

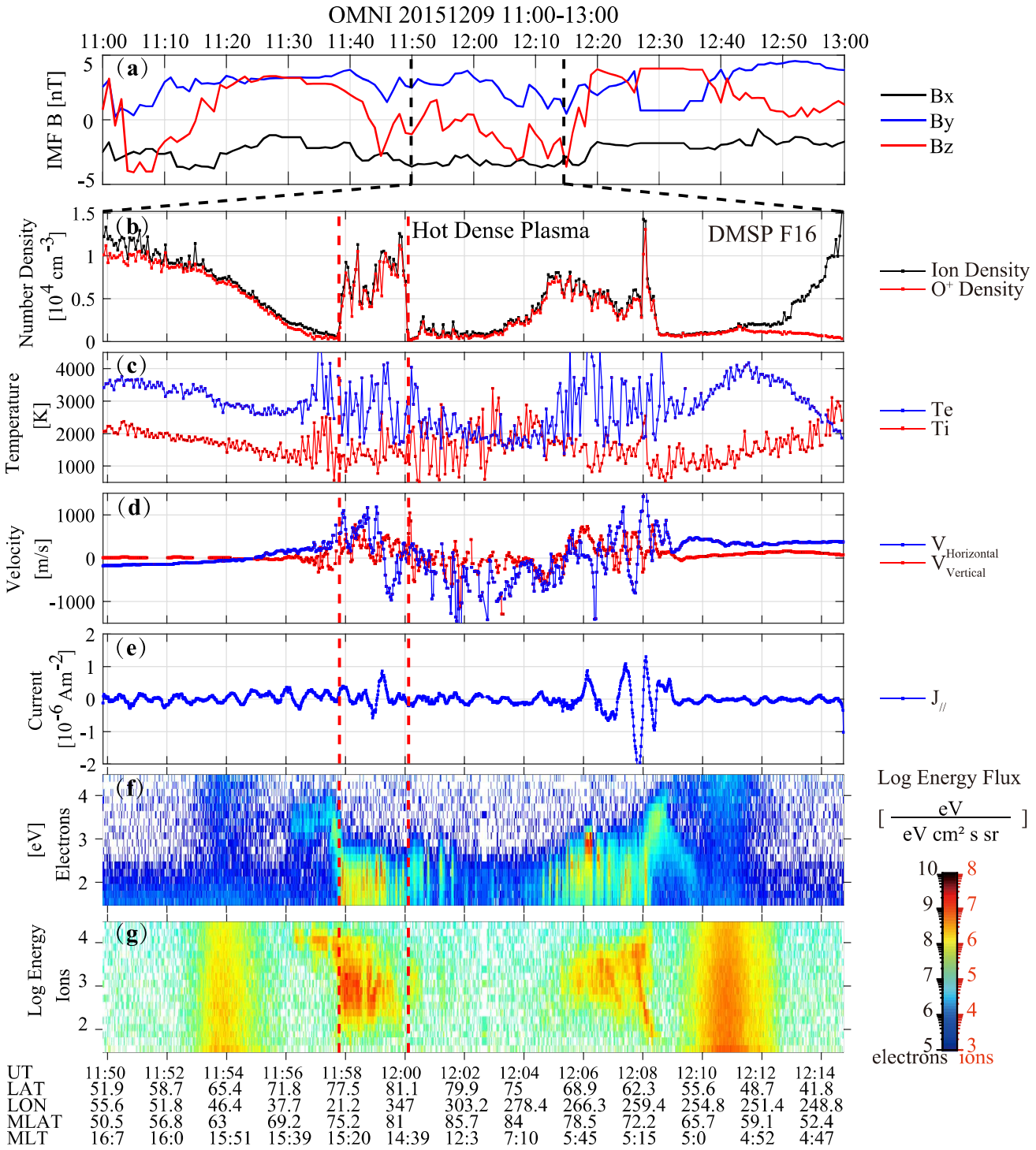

Figure 1. IMF data from OMNI and DMSP F16 data from a typical transit of the northern polar region on 9 December 2015 at 11:50~12:14 UT. The hot dense plasma is marked with the red dashed lines. From top to bottom, the panels show: (a) IMF Bx, By and Bz, (b) number density of ions and O+, (c) the electron and ion temperatures, (d) the horizontal velocity and vertical velocity, (e) the field-aligned current, and (f)–(g) the differential energy flux of precipitated electrons and ions.

S2). A clear trough is observed between dense plasma and the lower latitude high density region (Figure 1a2). Around 11:52–11:53 UT (Figure 2b1) the bright aurora started brightening further and expanded north-westward (Movie S1). The bright aurora continued to move northwest and became a PMAF (Oksavik et al., 2005, 2015; Sandholt et al., 1998, 2004). Several minutes later (Figure 2c1), DMSP F16 (the red/black star) crossed the

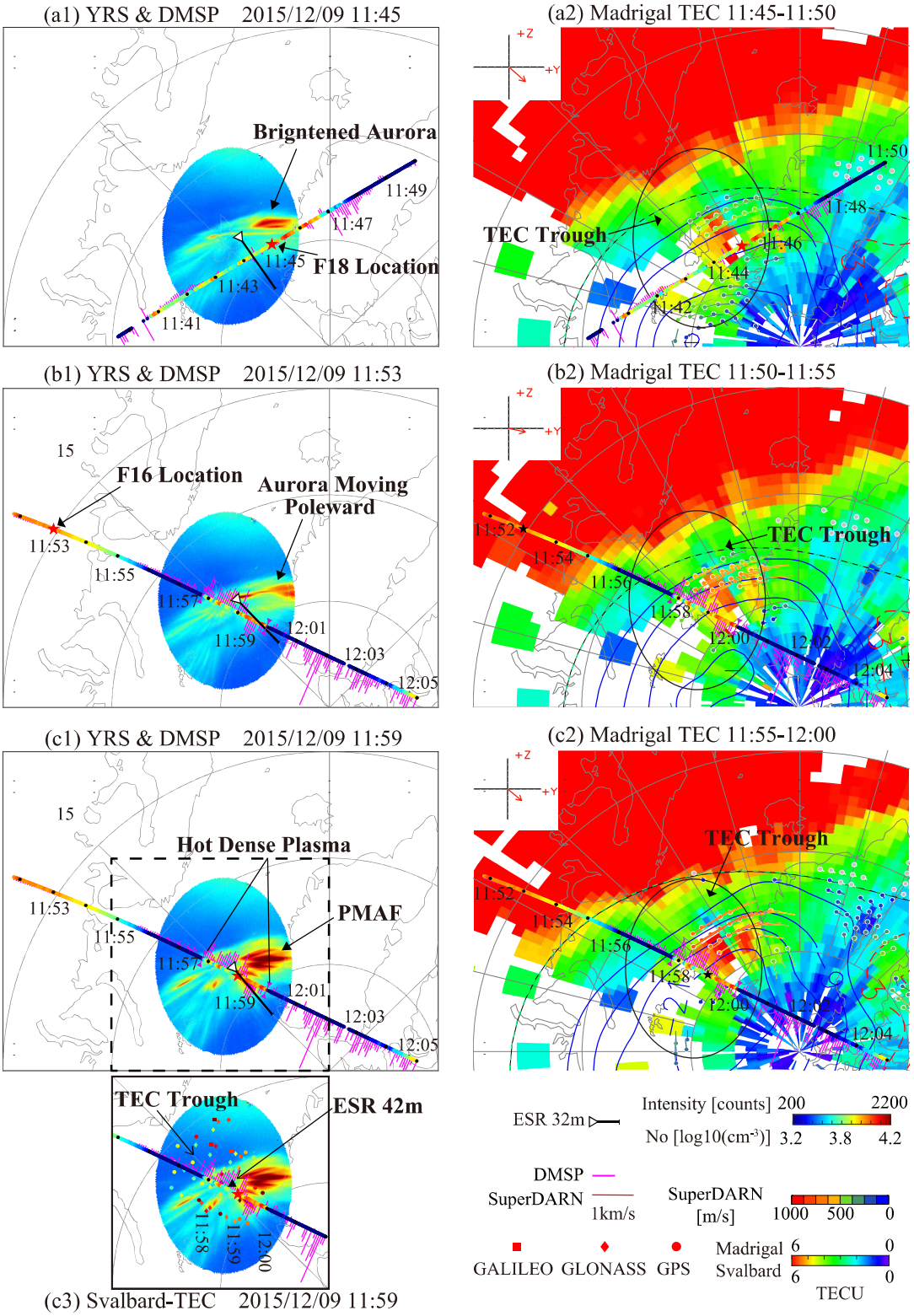

Figure 2. (a1–c1) Sequence of 630.0 nm all-sky images from the Chinese Yellow River Station, which are overlayed with the DMSP F16 and F18 trajectories and the ESR 32m & 42m beam locations. The color on top of the DMSP trajectory shows the number density of O+ (No), and the magenta line shows the horizontal ion velocity. (a3–b3) Sequence of Madrigal TEC and SuperDARN convection map data, respectively. (c3) 1-min TEC data from four GNSS receivers operated by the University of Bergen. Each symbol indicates the satellite system: GALILEO (square), GLONASS (diamond), and GPS (circle).

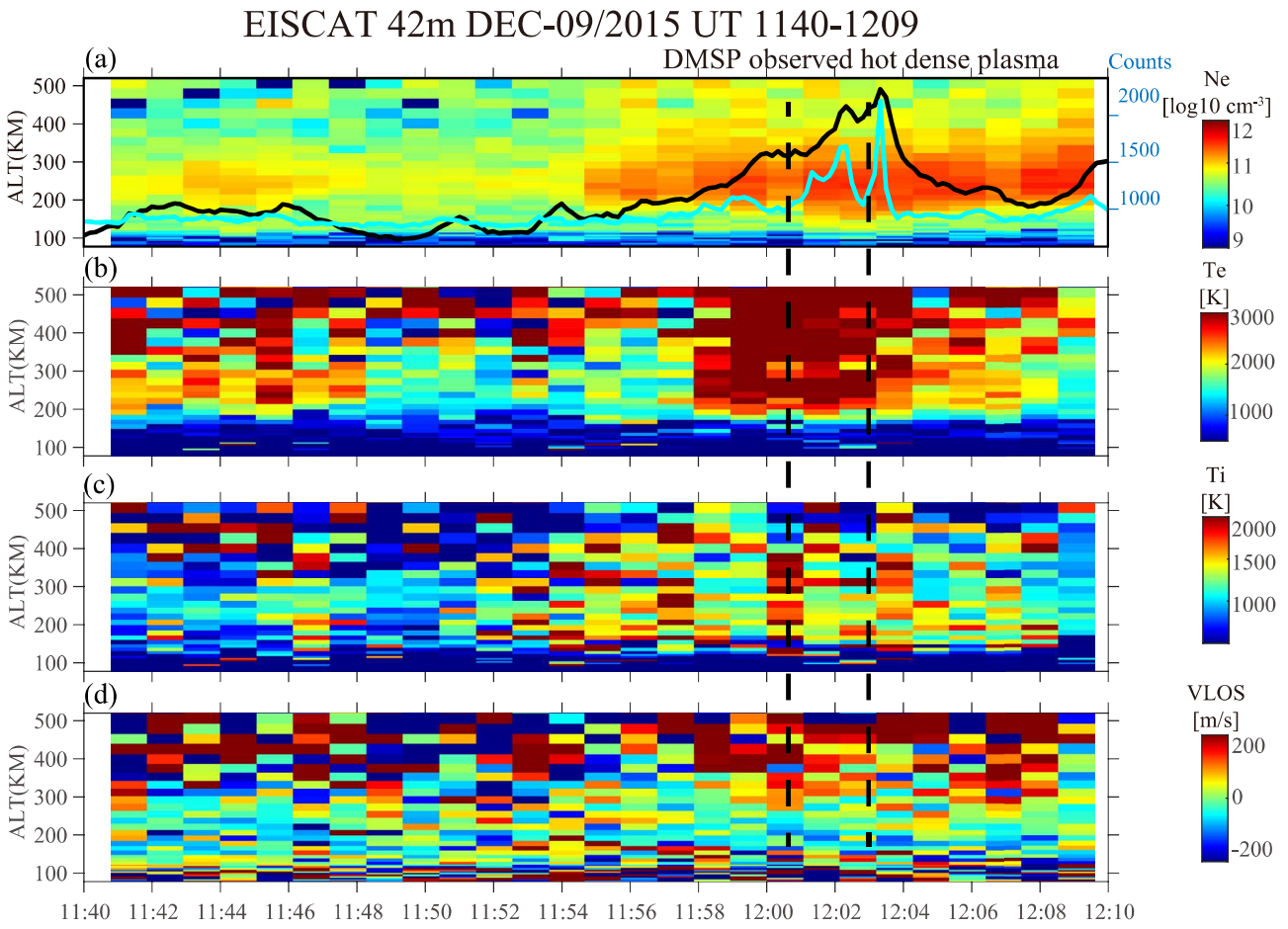

Figure 3. Time-series of EISCAT Svalbard Radar 42m antenna observations. From top to bottom each panel shows: (a) electron density, (b) electron temperature, (c) ion temperature, and (d) line-of-sight velocity. In each panel the altitude is shown along the left axis. The auroral intensity of 630.0 nm (red) and 557.7 nm (green) along the beam direction is shown in the top panel as black and blue lines, respectively. Note: The green line intensity has been doubled in the figure, for easier comparison.

auroral oval and captured the high ion density of the hot dense plasma. Meanwhile the PMAF intercepted the anti-sunward moving part of the hot dense plasma at 11:57–11:58 UT (Movie S1), indicating that these PMAFs were associated with dense plasma (Zhang et al., 2010). The ion and O^+ density in the anti-sunward part is much higher than that of the sunward part, suggesting that the enhanced precipitation may contribute to the increased density.

Although the PMAF expanded poleward after 11:53 UT, Figure 2b2-2c2 and Movie S3 show that the TEC trough always stayed between the hot dense plasma and the lower latitude dense plasma reservoir. Unfortunately, there were several data gaps in the Madrigal TEC data, so we also looked at the University of Bergen 1-min TEC data over Svalbard (Figure 2b3). These high-resolution data fill the data gap and confirm the TEC trough in the middle of the ASI FOV, and the lower latitude dense plasma reservoir extended 2° further poleward than in Figure 2c2. This suggests that the density source of the hot dense plasma should not be the lower latitude region.

To further investigate the plasma parameters and evolution of the hot dense plasma, ESR observations are shown in Figure 3. The figure shows ESR 42 m observations as a function of altitude along its magnetic-field aligned beam, with red and green line auroral missions overlaid as black and blue lines, respectively, in the top panel. Since the ESR 42 m antenna is ~50 km from the hot dense plasma (at about 11:58 UT), the radar observations make a close conjunction with the DMSP observation. At 11:48–11:54 UT, a low electron density, low electron and ion temperature region is observed associated with weak downward flow and weak auroral emission. Following the low-density region, a dense F region enters the radar field-of-view (FOV) and is accompanied by cold electron temperature and enhanced ion temperature at 11:55–11:58 UT. This cold and dense structure is not

associated with strong auroral emission, but shows similar plasma characteristics with those plasma observed by ESR 42 m at another MLT in auroral oval (such as 12:18 UT, 12:48 UT which is not shown). This suggest that they may be generated by the particle precipitation inside the auroral oval. After 11:58 UT, significant electron temperature and density enhancements are observed and are associated with enhanced auroral emission and upward flow, indicating the presence of particle precipitation. The enhancement of electron density and electron temperature are both below 180 km altitude. At 12:02 UT, when the auroral emission reaches its peak, the electron density between 140 and 180 km increases, but the electron temperature and the ion temperature seem unchanged. Comparing with Figure 2b1, the dense, hot plasma after 11:58 UT is associated with the PMAFs, and may be the equatorward part or the previous phase of the hot dense plasma. ESR 32 m antenna pointed toward it and also observed continuous F region density enhancements between 78° and 81° MLAT associated with electron temperature enhancement around 200 km during this time (not shown), which confirms the ESR 42m observation.

Here we summarize the characteristics of this hot dense plasma: Enhanced density structure is observed in the F region and at 800 km. The radar and satellite observed electron temperature enhancement when crossing the hot dense plasma. The velocity shows that the hot dense plasma is located around the flow reversal near the cusp. Equatorward of, and inside of the hot dense plasma, strong red auroral emissions are observed that move poleward like a PMAF. A clear TEC trough is observed between the lower latitude dense plasma reservoir and the hot dense plasma.

3.2. Event on 8 December 2013

On 8 December 2013 DMSP F16 crossed the polar cap region in the Northern Hemisphere at 10:29–10:52 UT. The IMF and in-situ plasma observations are shown in Figure 4, which is in a similar format to Figure 1. IMF By and Bz are weakly positive (<+2 nT), and IMF Bx is dominant and strong negative (around −5 nT); the solar wind density and velocity are 3 cm^{-3} and 620 km/s (Figure S1). A high-density plasma structure is highlighted by the red dashed lines at 10:37:22–10:39:14 UT; the average O^+ number density is about $2.88 \times 10^4 cm^{-3}$ and reaching up to $3.9 \times 10^4 cm^{-3}$ (Figure 4a). In the equatorward portion of this dense structure (before 10:38 UT), the electron temperature is a slightly higher than the ion temperature and associated with strong soft electron precipitation and fluctuating, mostly antisunward, horizontal flows. When the satellite moves further poleward (after ~10:38:20 UT), the precipitation of electrons reduces and the electron temperature decreases to the same level as the ion temperature, the horizontal velocity becomes continuously anti-sunward and ion precipitation is not observed (Figures 4d and 4f). The FACs are much weaker than for the previous event. These parameters suggest that this patch is a cold patch (Ma et al., 2018; Zhang et al., 2017).

To investigate the formation/evolution of this cold patch, Figure 5 is given in a similar format to Figure 2, but for the cold patch case on 8 December 2013. In each panel, strong cusp aurora emissions are observed in the middle of the ASI FOV which is crossed by the ESR 32m beam (black triangle and line). Dense along-track O^+ density and anti-sunward flow is observed by DMSP F18 when crossing ASI FOV at 10:11–10:16 UT, meanwhile a region of enhanced aurora is moving poleward. Enhanced electron temperature and strong particle precipitation suggests it could be a hot dense plasma (Figure S3). Figure 5a2 shows that the continuous dense TEC is accompanied with poleward convection at 11–13 MLT. Later, the DMSP F16 satellite first transits the left (eastern) part of the cusp aurora around 15 MLT, and then the satellite crosses the cold patch (marked by black lines) in a region free from optical emissions (Figure 5b1). Animations of the red and green line emissions are provided in Movies S4 and S5, respectively. From 10:13 to 10:38 UT, the northward moving aurora further expands poleward (or brighten in sequence) at 14 MLT, forms a north-south aligned auroral arc (the contour given by black lines) and finally connects with the equatorial edge of the cusp aurora (Movie S4), while the poleward expansion can also be observed in the green emission but is much weaker (Movie S5). The dominant radial IMF (Bx strongly negative) and its north-south orientation is characteristic of an auroral feature called throat aurora (Han et al., 2016). This poleward expansion of aurora also matches well with the TEC movement in Figure 5a2-5c2 and Movie S6, which suggest the auroral precipitation and dayside dense plasma may both contribute. DMSP F16 is right in the head of the TOI and is associated with strong O^+ density comes from the dusk side. This is also confirmed by 1-min University of Bergen TEC data in panel c3, indicating that the dayside solar EUV ionized plasma is a likely source of the cold patch (Moen, Qiu, et al., 2008; Zhang et al., 2013).

Figure 6 is in a similar format to Figure 3 but for the cold patch case. Since the ESR 32m beam sweeps zonally over the cold patch and the ESR 42m beam is far equatorward of the cold patch, only ESR 32m observations are shown in Figure 6. Most of time, the antenna keeps pointing to the south-west and outside of the cold patch region.

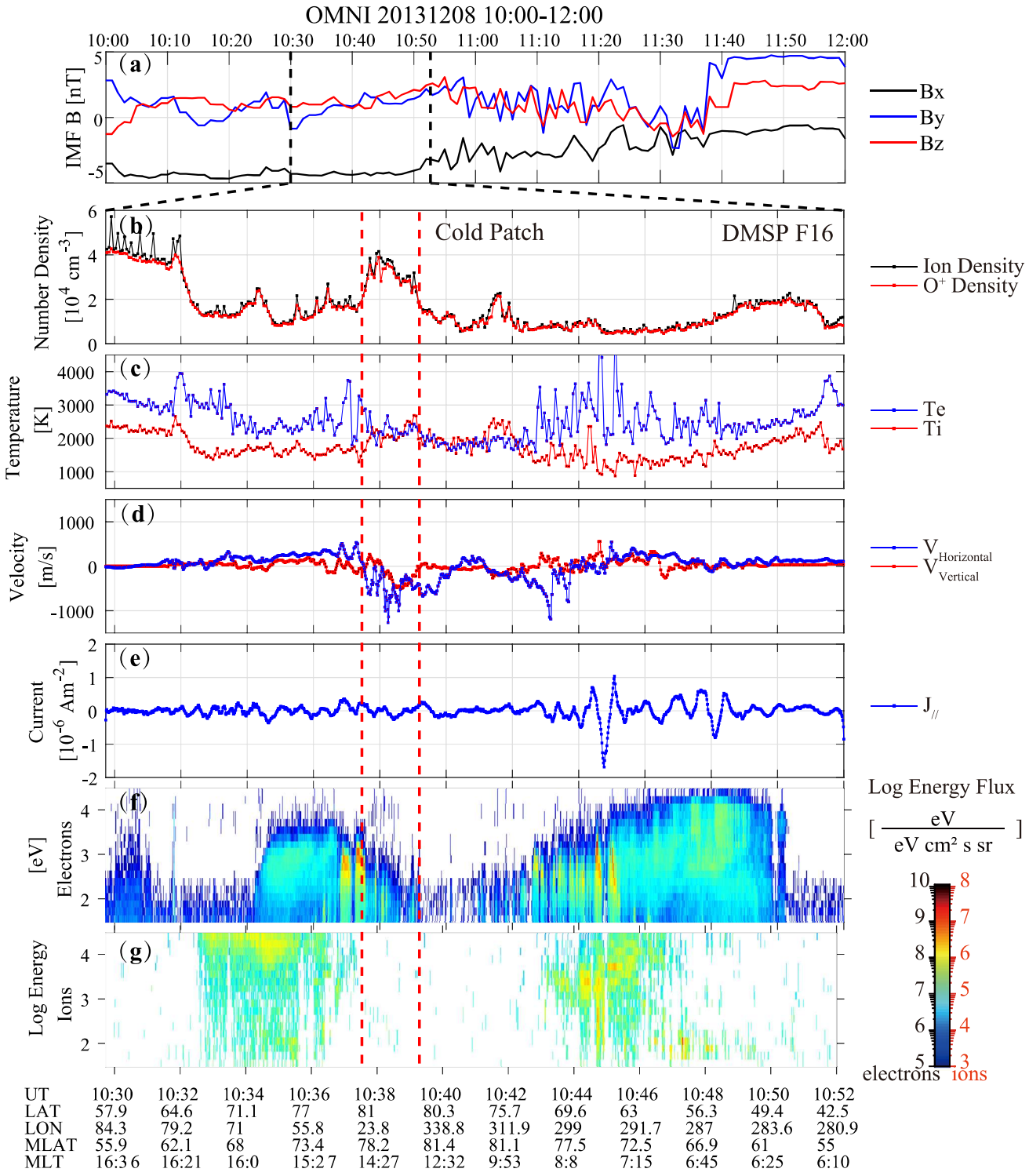

Figure 4. Similar format to Figure 1 but for the DMSP F16 transit on 8 December 2013 at 10:29~10:52 UT. The cold patch is marked with the red dashed lines.

The ASI and TEC map in Figure 5 suggest the ESR 32m antenna beam crossed the auroral oval and dense TEC, as confirmed by dense E-region (~140 km) and dense F region (>280 km) which is associated with enhanced red and green band aurora emissions (black and blue line in 6a). Meanwhile the electron and ion temperature are also enhanced to ~2,900 K and over 2,000 K, respectively. These hot plasmas move sunward (equatorward) toward

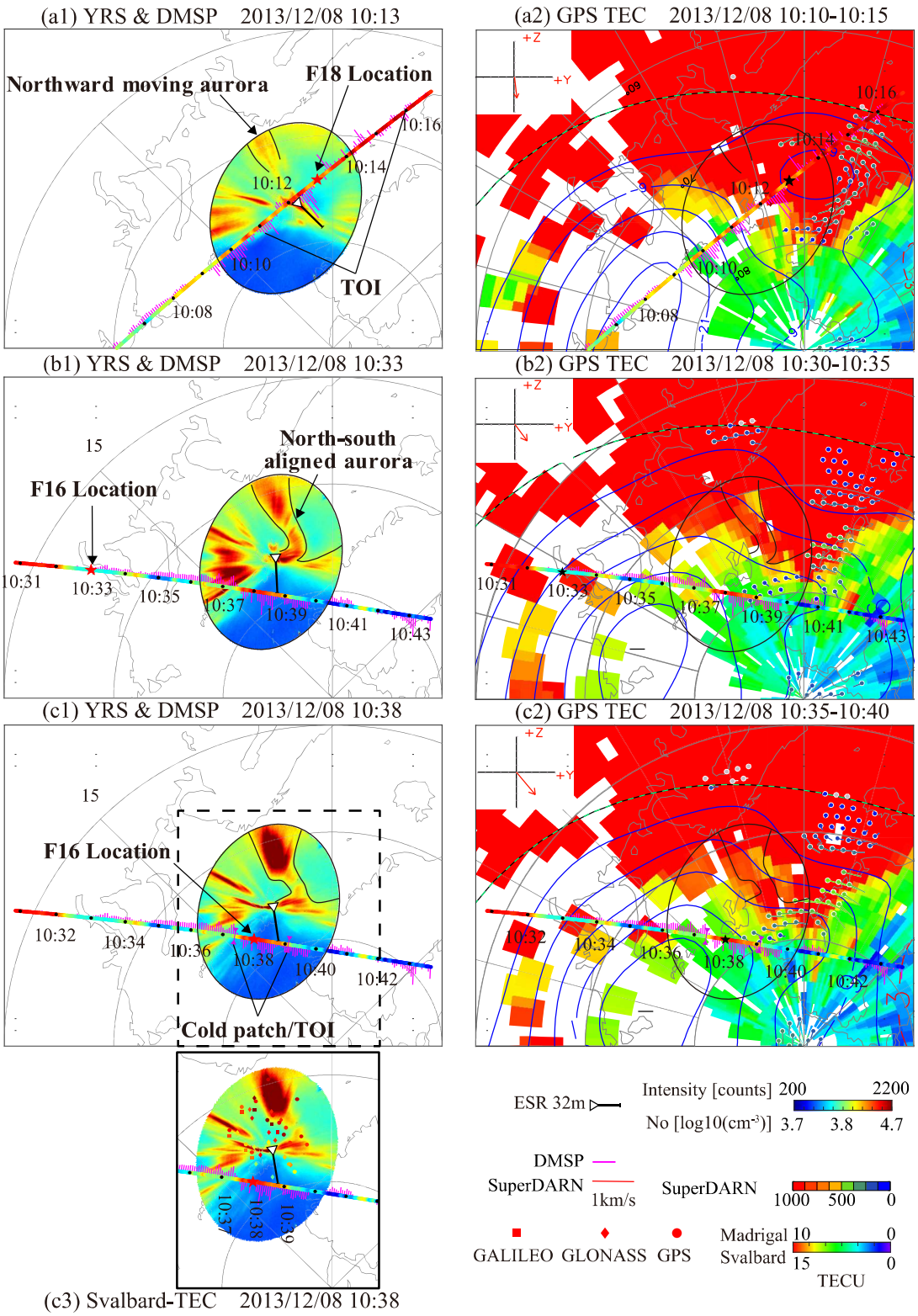

Figure 5. Similar format to Figure 2 but for the cold patch case on 8 December 2013. The locations of the DMSP F16 satellite are marked by red/black stars.

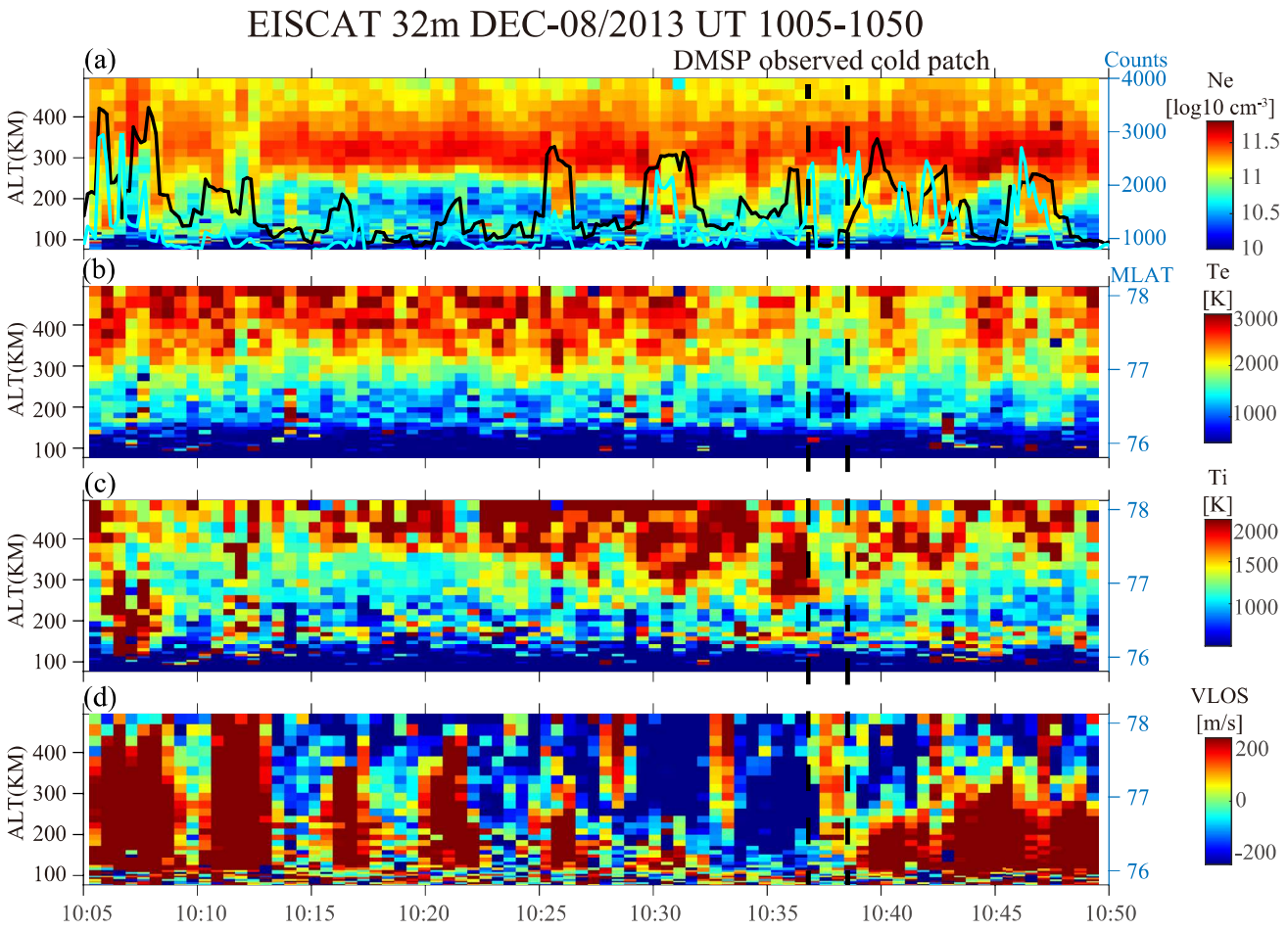

Figure 6. Time-series plot of EISCAT Svalbard Radar 32m antenna observations. From top to bottom each panel shows: (a) electron density, (b) electron temperature, (c) ion temperature, and (d) line-of-sight ion velocity. In each panel the altitude is along the left axis, and the magnetic latitude MLAT is shown along the right axis.

the radar. The antenna points to the location of cold patch three times at 10:28, 10:33, and 10:38 UT, and the DMSP crossing is marked by dash lines. During each of these periods strong anti-sunward velocity (poleward) is observed with decayed E region, the red and green aurora is very weak, and the electron and ion temperatures are cooler (less than 2000 K) compared with surrounding regions. Compare with the sequence plots in Figure 5, it is suggested that this cold and dense plasma is the poleward part of TOI in the polar cap, and it had experienced particle precipitation in auroral oval after being transported from the sunlit region. These parameters of this cold, dense plasma is similar to those of the "polar cap patch" observed by the ESR 32m and Tromsø VHF radars (Carlson, 2012; Zhang et al., 2011).

In summary, the cold patch is associated with enhanced ion/electron density above ~280 km, which may originate from a lower latitude solar ionized reservoir. The cold patch is accompanied by anti-sunward flow in a region equatorward of the cusp, where there is a lack of particle precipitation. The ion and electron temperatures of the cold patch are at the same level as seen by the DMSP satellite at 800 km altitude, whereas the electrons are cooler than the ions between 170 and 220 km but become warmer than ions at higher altitude.

4. Discussion

In the above two cases, both the hot dense plasma and cold patches are accompanied by auroral forms (PMAF and throat aurora) in the cusp region. Their spatial extent is about 700–900 km (based on DMSP observation) and are associated with anti-sunward flow between two widely distributed sunward flows. These phenomena have strong flow shears that in magnitude are similar to the Reversed Flow Events (RFE) reported by Rinne

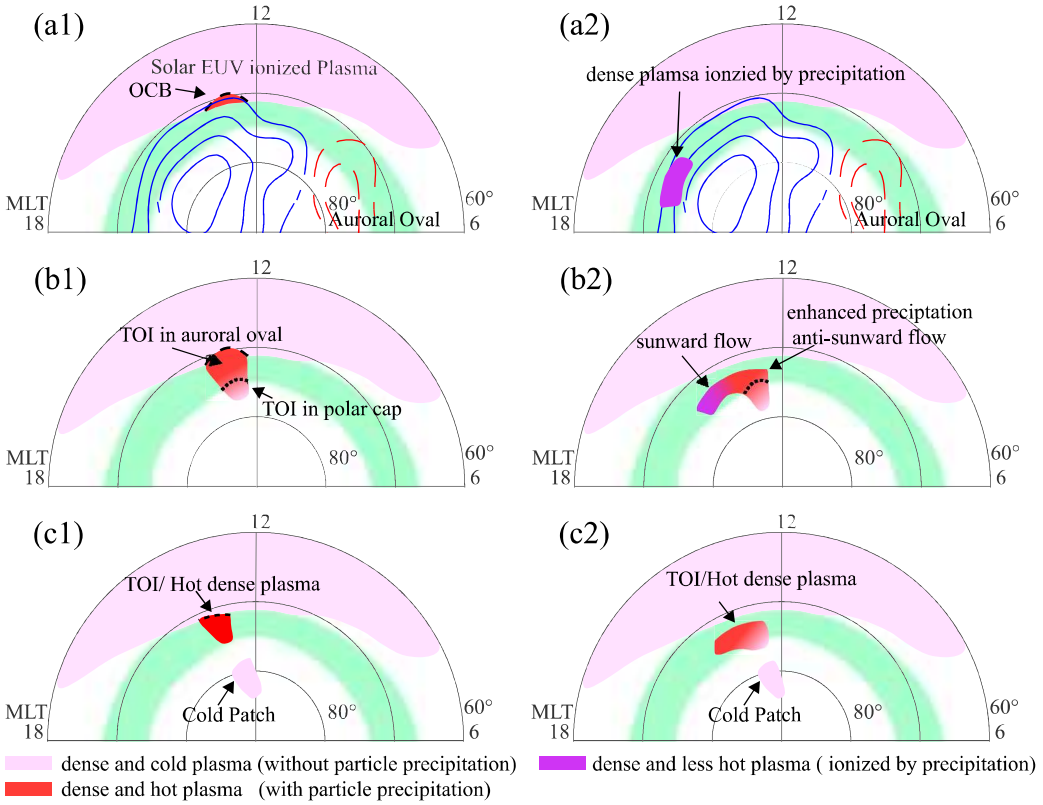

Figure 7. Sketches of the evolution of TOI and polar cap patches. The pink region indicates the solar EUV ionized dense plasma reservoir (dense and cold plasma) at middle latitudes. The dense and hot plasma associated with particle precipitation is marked in red color. The plasma ionized by auroral precipitation is marked in purple color. The auroral oval is marked by the green color.

et al. (2007), where the mesoscale plasma flow is in the opposite direction to the large-scale background flow in a ~200 km wide region. RFEs have been suggested to be the ionospheric signature of a flux transfer event (FTE) at the magnetopause and is also associated with a PMAF (Moen, Rinne, et al., 2008; Oksavik et al., 2011; Southwood, 1987). Hwang et al. (2020) report a patch-like density enhancement when an FTE-associated PMAF moves poleward and decays. The transient magnetic reconnection due to the FTE can lead to equatorward erosion of the open-closed boundary into a lower latitude reservoir of higher density plasma. The intensified poleward flows will transport high-density plasma into the polar cap in the form of a polar cap patch (Lockwood & Carlson, 1992; Zhang et al., 2011). Our observations (Figures 2 and 4) fully agree with this process where auroral forms and patches are distributed in a low-to-high latitude sequence that propagates poleward into the polar cap.

In the past, the polar cap patch is defined as a dense structure in the polar cap and its class whether "hot" or "cold" depending on the space/ground-based observations (Zhang et al., 2017). The statistics work done by Ma et al. (2018) and Zhang et al. (2022) suggest the hot patch is located equatorward of cold patch, and suggest the particle precipitation and transport process may dominate the hot and cold patch formation, respectively. This study claim that these mechanisms can both contribute the formation of patches. In Figure 7 we show a sketch of the formation and evolution of dense plasma across the auroral oval (green area) and into the polar cap. The pink and red area indicate the hot-dense plasma and the cold-dense plasma, respectively. The convection lines (blue solid and red dashed lines) are modified from the SuperDARN convection map at 10:36 UT on 8 December 2013. There are two evolution processes described in panel a1-c1 and a2-c2, which correspond to 2013 case and 2015 case, respectively.

In the first stage of panels a1-c1 (panel 7a1), enhanced dayside magnetic reconnection will cause the open/close boundary (OCB) to migrate equatorward into the solar EUV ionized plasma reservoir at lower latitudes. This will result in the drag of the dense plasma into the anti-sunward convection, leading to its entry into the auroral oval

(panel 7b1). As a result of auroral particle precipitation, the dense plasma will be heated and their electron density will increase, transforming it into a warmer TOI than previous. Additionally, the equatorward boundary of the cusp may display brightening of the poleward moving auroal forms (Carlson et al., 2004; Fasel, 1995; Han et al., 2017; Hwang et al., 2020; Xing et al., 2012). The equatorward portion of the TOI is located within the auroral oval and is characterized by particle precipitation and enhanced electron temperature resulting from the newly open flux. Conversely, the poleward portion of the TOI is situated on old open flux in the polar cap and the precipitation is in a state of decay, its electron temperature will gradually decease (Herlingshaw et al., 2019, 2020, 2022; Sandholt & Farrugia, 2009). When the IMF By changes orientation, the modified convection will "cut off" the continuous TOI (Zhang et al., 2013). The poleward part will remain in the polar cap and turns from hot dense plasma (or hot patch) to cold patch after the precipitation runs out and electron temperature cools down. While the equatorward part will be a warmer TOI/hot dense plasma due to the sufficient precipitation in the auroral oval (panel 7c1).

In panels a2-c2, dense plasma can be generated by particle precipitation within the auroral oval (panel 7a2), and move sunward along the convection. When an auroral structure, such as throat aurora or PMAF, contact with these dense plasma, the associated enhanced particle precipitation will heat, ionize the dense plasma and pull them further poleward (Nishimura et al., 2014). Consequently, a hot similar to 7b1 is formed in panel 7b2. The portions still within the auroral oval will be hot and dense, while those already within the polar cap will be dense but less hot. If any cut-off process occurs, the poleward, less hot portion of the TOI will be segmented and undergo the process of transforming from a hot patch to a cold patch.

5. Conclusions

In this study, we have analyzed two polar cap patch events consisting of DMSP observations at ~800 km, ESR observations at 80–500 km, and ASI observations of 557.7 and 630.0 nm at the Chinese Yellow River Station in Svalbard, in order to better understand the differences and similarities between the hot and cold patches. Our key findings are the following.

1. Compared with surrounding regions, the plasma density and TEC were both enhanced in hot and cold patches. For the cold patch, the electron and ion temperatures were at the same level, with no auroral emission and in anti-sunward flow. For the hot dense plasma/hot patch, strong particle precipitation and auroral emissions were observed and were associated with electron temperature enhancement, which is about ~1,000 K higher than the ion temperature. A flow reversal was observed inside and the field-aligned current was enhanced.
2. Inside the cusp region, auroral forms (PMAF or throat aurora) were seen equatorward of both type of patches, which were associated with narrow anti-sunward flows in between two regions of sunward flow. This suggests that the formation or development of both types of patches may be associated with transient dayside reconnection.
3. Enhanced TEC was observed in both types of patches. The transport process of dense plasma from a lower latitude sunlit reservoir, and particle precipitation in the auroral oval might both contribute to the formation or development of cold/hot patch. The hot dense plasma was accompanied by local auroral emission and particle precipitation, suggesting that the auroral particle precipitation also contributed to its development.
4. We propose that in some situations the cold and hot patches may be the same density feature but in different phases of its development. When a transient auroral feature (PMAF or throat aurora) begins to form and propagate poleward with dense solar EUV ionized plasma or dense ionized plasma in the auroral oval, it may first appear as a hot dense plasma (or a warmer TOI). When the particle precipitation later reduces, the electron temperature may drop to the same level as the ion temperature, which would qualify it to be classified as a cold patch.

Data Availability Statement

The DMSP velocity, density, temperature and energy spectrum data were obtained from National Centers for Environmental Information (https://www.ncei.noaa.gov/data/dmsp-space-weather-sensors/access/). The red band and green band aurora emission data of Yellow River Station all sky imager can be obtained from https://doi.org/10.5281/zenodo.7672302 (Ma et al., 2023). We acknowledge the use of SuperDARN convection data. The authors acknowledge the use of SuperDARN data. SuperDARN is a collection of radars funded by national scientific funding agencies of Australia, Canada, China, France, Italy, Japan, Norway, South Africa, United Kingdom, and the United States of America. SuperDARN convection map data is obtained from https://superdarn.ca/ascii-download. The GPS-TEC and ESR 32m & 42m are obtained from the Madrigal database (http://cedar.openmadrigal.org/ftp/). The 1-min TEC data over Svalbard is part of the University of Bergen Global Navigation Satellite System Data Collection (Oksavik, 2020a, 2020b).

Acknowledgments
This work was supported by the National Natural Science Foundation of China (Grants 42204164, 42120104003 and 42074188), the Chinese Meridian Project, the China Postdoctoral Science Foundation (Grant 2021M701974), the Stable-Support Scientific Project of China Research Institute of Radiowave Propagation (Grant A132101W02), the International Partnership Program of Chinese Academy of Sciences (Grant 183311KYSB20200003), the Shandong Provincial Natural Science Foundation (grant ZR2022QD077, ZR2022MD034), the foundation of National Key Laboratory of Electromagnetic Environment (Grant 6142403180204) and Research Council of Norway under contract 223252.

References

Baker, K. B., & Wing, S. (1989). A new coordinate system for conjugate studies at high latitudes. *Journal of Geophysical Research*, *94*(A7), 9139–9143. https://doi.org/10.1029/JA094iA07p09139

Carlson, H. C. (2012). Sharpening our thinking about polar cap ionospheric patch morphology, research, and mitigation techniques. *Radio Science*, *47*(4), RS0L21. https://doi.org/10.1029/2011RS004946

Carlson, H. C., Moen, J., Oksavik, K., Nielsen, C. P., McCrea, I. W., Pedersen, T. R., & Gallop, P. (2006). Direct observations of injection events of subauroral plasma into the polar cap. *Geophysical Research Letters*, *33*(5), L05103. https://doi.org/10.1029/2005GL025230

Carlson, H. C., Oksavik, K., Moen, J., & Pedersen, T. (2004). Ionospheric patch formation: Direct measurements of the origin of a polar cap patch. *Geophysical Research Letters*, *31*(8), L08806. https://doi.org/10.1029/2003GL018166

Crowley, G. (1996). A critical review of ionospheric patches and blobs. In *Review of radio science 1993–1996* (pp. 619–648). Oxford University Press.

Fasel, G. J. (1995). Dayside poleward moving auroral forms: A statistical study. *Journal of Geophysical Research*, *100*(A7), 11891–11905. https://doi.org/10.1029/95JA00854

Goodwin, L. V., Iserhienrhien, B., Miles, D. M., Patra, S., Van der Meeren, C., Buchert, S. C., et al. (2015). Swarm in situ observations of F region polar cap patches created by cusp precipitation. *Geophysical Research Letters*, *42*(4), 996–1003. https://doi.org/10.1002/2014GL062610

Han, D.-S., Chen, X.-C., Nishimura, Y., Lyons, L. R., Liu, J.-J., Hu, H.-Q., et al. (2017). Observational properties of dayside throat aurora and implications on the possible generation mechanisms. *Journal of Geophysical Research: Space Physics*, *122*(2), 1853–1870. https://doi.org/10.1002/2016JA023394

Han, D.-S., Nishimura, Y., Lyons, L. R., Hu, H.-Q., & Yang, H.-G. (2016). Throat aurora: The ionospheric signature of magnetosheath particles penetrating into the magnetosphere. *Geophysical Research Letters*, *43*(5), 1819–1827. https://doi.org/10.1002/2016GL068181

Hardy, D. A., Schmitt, L. K., Gussenhoven, M. S., Marshall, F. J., & Yeh, H. C. (1984). *Precipitating electron and ion detectors (SSJ/4) for the block 5D/flights 6-10 DMSP (Defense Meteorological Satellite Program) satellites: Calibration and data presentation. Rep. AFGL-TR-84-0317. Air Force Geophys*. Lab., Hanscom Air Force Base.

Herlingshaw, K., Baddeley, L., Oksavik, K., Lorentzen, D., & Laundal, K. (2022). A statistical study of polar cap flow channels observed in both hemispheres using SuperDARN radars. *J. Space Weather Space Climate*, *12*, 39. https://doi.org/10.1051/swsc/2022037

Herlingshaw, K., Baddeley, L. J., Oksavik, K., & Lorentzen, D. A. (2020). A statistical study of polar cap flow channels and their IMF by dependence. *Journal of Geophysical Research: Space Physics*, *125*(11), e2020JA028359. https://doi.org/10.1029/2020JA028359

Herlingshaw, K., Baddeley, L. J., Oksavik, K., Lorentzen, D. A., & Bland, E. C. (2019). A study of automatically detected flow channels in the polar cap ionosphere. *Journal of Geophysical Research: Space Physics*, *124*(11), 9430–9447. https://doi.org/10.1029/2019JA026916

Hu, Z. J., Yang, H., Huang, D., Araki, T., Sato, N., Taguchi, M., et al. (2009). Synoptic distribution of dayside aurora: Multiple-wavelength all-sky observation at Yellow River Station in Ny-Ålesund, Svalbard. *Journal of Atmospheric and Solar-Terrestrial Physics*, *71*(8–9), 794–804. 794–804 Hwang 2020. https://doi.org/10.1016/j.jastp.2009.02.010

Hwang, K.-J., Nishimura, Y., Coster, A. J., Gillies, R. G., Fear, R. C., Fuselier, S. A., et al. (2020). Sequential observations of flux transfer events, poleward-moving auroral forms, and polar cap patches. *Journal of Geophysical Research: Space Physics*, *125*(6), e2019JA027674. https://doi.org/10.1029/2019JA027674

Lockwood, M., & Carlson, H. C. (1992). Production of polar cap electron density patches by transient magnetopause reconnection. *Geophysical Research Letters*, *19*(17), 1731–1734. https://doi.org/10.1029/92GL01993

Lockwood, M., Davies, J. A., Moen, J., Van Eyken, A. P., Oksavik, K., McCrea, I. W., & Lester, M. (2005). Motion of the dayside polar cap boundary during substorm cycles: II. Generation of poleward-moving events and polar cap patches by pulses in the magnetopause reconnection rate. *Ann. Geophys.*, *23*(11), 3513–3532. https://doi.org/10.5194/angeo-23-3513-2005

Lockwood, M., McCrea, I. W., Milan, S. E., Moen, J., Cerisier, J. C., & Thorolfsson, A. (2000). Plasma structure within poleward-moving cusp-cleft auroral transients: EISCAT Svalbard radar observations and an explanation in terms of large local time extent of events. *Ann. Geophys.*, *18*(9), 1027–1042. https://doi.org/10.1007/s00585-000-1027-5

Lorentzen, D. A., Moen, J., Oksavik, K., Sigernes, F., Saito, Y., & Johnsen, M. G. (2010). In situ measurement of a newly created polar cap patch. *Journal of Geophysical Research*, *115*(A12), a–n. https://doi.org/10.1029/2010ja015710

Ma, Y.-Z., Zhang, Q.-H., Jayachandran, P. T., Oksavik, K., Lyons, L. R., Xing, Z.-Y., et al. (2020). Statistical study of the relationship between ion upflow and field-aligned current in the topside ionosphere for both hemispheres during geomagnetic disturbed and quiet time. *Journal of Geophysical Research: Space Physics*, *125*(9), e2019JA027538. https://doi.org/10.1029/2019JA027538

Ma, Y.-Z., Zhang, Q.-H., Lyons, L. R., Oksavik, K., Xing, Z.-Y., Hairston, M. R., et al. (2023). Yellow River ASI data for cold patch and hot patch events [Dataset]. Zenodo. https://doi.org/10.5281/zenodo.7672302

Ma, Y.-Z., Zhang, Q.-H., Xing, Z.-Y., Heelis, R. A., Oksavik, K., & Wang, Y. (2018). Theion/electron temperature characteristics of polar cap classical and hot patches and their influence on ion upflow. *Geophysical Research Letters*, *45*(16), 8072–8080. https://doi.org/10.1029/2018GL079099

MacDougall, J., & Jayachandran, P. T. (2007). Polar patches: Auroral zone precipitation effects. *Journal of Geophysical Research*, *112*(A5), A05312. https://doi.org/10.1029/2006ja011930

Milan, S. E., Lester, M., & Yeoman, T. K. (2002). HF radar polar patch formation revisited: Summer and winter variations in dayside plasma structuring. *Ann. Geophys.*, *20*(4), 487–499. https://doi.org/10.5194/angeo-20-487-2002

Moen, J., Qiu, X. C., Carlson, H. C., Fujii, R., & McCrea, I. W. (2008). On the diurnal variability in F2-region plasma density above the EISCAT Svalbard radar. *Ann. Geophys.*, *26*(8), 2427–2433. https://doi.org/10.5194/angeo-26-2427-2008

Moen, J., Rinne, Y., Carlson, H. C., Oksavik, K., Fujii, R., & Opgenoorth, H. (2008). On the relationship between thin Birkeland current arcs and reversed flow channels in the winter cusp/cleft ionosphere. *Journal of Geophysical Research*, *113*(A9), A09220. https://doi.org/10.1029/2008JA013061

Newell, P. T., Wing, S., Meng, C.-I., & Sigillito, V. (1991). The auroral oval position, structure, and intensity of precipitation from 1984 onward: An automated on-line data base. *Journal of Geophysical Research*, *96*(A4), 5877–5882. https://doi.org/10.1029/90JA02450

Nishimura, Y., Lyons, L. R., Zou, Y., Oksavik, K., Moen, J. I., Clausen, L. B., et al. (2014). Day-night coupling by a localized flow channel visualized by polar cap patch propagation. *Geophysical Research Letters*, *41*(11), 3701–3709. https://doi.org/10.1002/2014gl060301

Nishimura, Y., Sadler, F. B., Varney, R. H., Gilles, R., Zhang, S. R., Coster, A. J., et al. (2021). Cusp dynamics and polar cap patch formation associated with a small IMF southward turning. *Journal of Geophysical Research: Space Physics*, *126*(5), e2020JA029090. https://doi.org/10.1029/2020JA029090

Oksavik, K. (2020a). Documentation of GNSS total electron content and Scintillation data (60 s) at Svalbard [dataset], DataverseNO, V1. https://doi.org/10.18710/EA5BYX

Oksavik, K. (2020b). The University of Bergen Global Navigation satellite system data collection [dataset]. DataverseNO. https://doi.org/10.18710/AJ4S-X394

Oksavik, K., Moen, J., Carlson, H. C., Greenwald, R. A., Milan, S. E., Lester, M., & Barnes, R. J. (2005). Multi-instrument mapping of the small-scale flow dynamics related to a cusp auroral transient. *Annales Geophysicae*, *23*(7), 2657–2670.

Oksavik, K., Moen, J. I., Rekaa, E. H., Carlson, H. C., & Lester, M. (2011). Reversed flow events in the cusp ionosphere detected by SuperDARN HF radars. *Journal of Geophysical Research*, *116*(A12), A12303. https://doi.org/10.1029/2011JA016788

Oksavik, K., Ruohoniemi, J. M., Greenwald, R. A., Baker, J. B. H., Moen, J., Carlson, H. C., et al. (2006). Observations of isolated polar cap patches by the European incoherent scatter (EISCAT) Svalbard and super dual auroral radar network (SuperDARN) Finland radars. *Journal of Geophysical Research*, *111*(A5), A05310. https://doi.org/10.1029/2005JA011400

Oksavik, K., Van der Meeren, C., Lorentzen, D. A., Baddeley, L. J., & Moen, J. (2015). Scintillation and loss of lock from poleward moving auroral forms in the cusp ionosphere. *Journal of Geophysical Research: Space Physics*, *120*(10), 9161–9175. https://doi.org/10.1002/2015JA021528

Pitout, F., & Blelly, P. (2003). Electron density in the cusp ionosphere: Increase or depletion? *Geophysical Research Letters*, *30*(14), 1726. https://doi.org/10.1029/2003GL017151

Rich, F. J., & Hairston, M. (1994). Large-scale convection patterns observed by DMSP. *Journal of Geophysical Research*, *99*(A3), 3827–3844. https://doi.org/10.1029/93JA03296

Rinne, Y., Moen, J., Oksavik, K., & Carlson, H. C. (2007). Reversed flow events in the winter cusp ionosphere observed by the European Incoherent Scatter (EISCAT) Svalbard radar. *Journal of Geophysical Research*, *112*(A10), A10313. https://doi.org/10.1029/2007JA012366

Rodger, A. S., Pinnock, M., Dudeney, J. R., Baker, K. B., & Greenwald, R. A. (1994). A new mechanism for polar patch formation. *Journal of Geophysical Research*, *99*(A4), 6425–6436. https://doi.org/10.1029/93JA01501

Sandholt, P., & Farrugia, C. (2009). Plasma flow channels at the dawn/dusk polar cap boundaries: Momentum transfer on old open field lines and the roles of IMF by and conductivity gradients. *Annales Geophysicae*, *728 27*(4), 1527–1554. https://doi.org/10.5194/angeo-27-1527-2009

Sandholt, P. E., Denig, W. F., Farrugia, C. J., Lybekk, B., & Trondsen, E. (2002). Auroral structure at the cusp equatorward boundary: Relationship with the electron edge of low-latitude boundary layer precipitation. *Journal of Geophysical Research*, *107*(A9), 1235. https://doi.org/10.1029/2001JA005081

Sandholt, P. E., Farrugia, C. J., & Denig, W. F. (2004). Dayside aurora and the role of IMF |By|/|Bz|: Detailed morphology and response to magnetopause reconnection. *Ann. Geophys.*, *22*(2), 613–628. https://doi.org/10.5194/angeo-22-613-2004

Sandholt, P. E., Farrugia, C. J., Moen, J., Noraberg, Ø., Lybekk, B., Sten, T., & Hansen, T. (1998). A classification of dayside auroral forms and activities as a function of interplanetary magnetic field orientation. *Journal of Geophysical Research*, *103*(A10), 23325–23345. https://doi.org/10.1029/98JA02156

Southwood, D. J. (1987). The ionospheric signature of flux-transfer events. *Journal of Geophysical Research*, *92*(A4), 3207–3213. https://doi.org/10.1029/JA092iA04p03207

Xing, Z. Y., Yang, H. G., Han, D. S., Wu, Z. S., J Hu, Z., Zhang, Q. H., et al. (2012). Poleward moving auroral forms (PMAFs) observed at the Yellow River Station: A statistical study of its dependence on the solar wind conditions. *Journal of Atmospheric and Solar-Terrestrial Physics*, *86*, 25–33. https://doi.org/10.1016/j.jastp.2012.06.004

Zhang, D., Zhang, Q.-H., Ma, Y.-Z., Oksavik, K., Lyons, L. R., Xing, Z.-Y., et al. (2022). The dependence of cold and hot patches on local plasma transport and particle precipitation in Northern Hemisphere winter. *Geophysical Research Letters*, *49*(12), e2022GL098671. https://doi.org/10.1029/2022GL098671

Zhang, D., Zhang, Q.-H., Ma, Y.-Z., Oksavik, K., Lyons, L. R., Zhang, Y.-L., et al. (2021). Solar and geomagnetic activity impact on occurrence and spatial size of cold and hot polar cap patches. *Geophysical Research Letters*, *48*(18), e2021GL094526. https://doi.org/10.1029/2021GL094526

Zhang, Q.-H., Dunlop, M. W., Lockwood, M., Liu, R. Y., Hu, H. Q., Yang, H. G., et al. (2010). Simultaneous observations of reconnection pulses at cluster and their effects on the cusp aurora observed at the Chinese Yellow River Station. *Journal of Geophysical Research*, *115*(A10), A10237. https://doi.org/10.1029/2010JA015526

Zhang, Q.-H., Lockwood, M., Foster, J. C., Zhang, S.-R., Zhang, B.-C., McCrea, I. W., et al. (2015). Direct observations of the full Dungey convection cycle in the polar ionosphere for southward interplanetary magnetic field condition. *Journal of Geophysical Research: Space Physics*, *120*(6), 4519–4530. https://doi.org/10.1002/2015JA021172

Zhang, Q.-H., Ma, Y.-Z., Jayachandran, P. T., Moen, J., Lockwood, M., Zhang, Y.-L., et al. (2017). Polar cap hot patches: Enhanced density structures s different from the classical patches in the ionosphere. *Geophysical Research Letters*, *44*(16), 8159–8167. https://doi.org/10.1002/2017GL073439

Zhang, Q.-H., Zhang, B.-C., Hu, H.-Q., Moen, J., Lockwood, M., McCrea, I. W., et al. (2013). Polar cap patch segmentation of the tongue of ionization in the morning convection cell. *Geophysical Research Letters*, *40*(12), 2918–2922. https://doi.org/10.1002/grl.50616

Zhang, Q.-H., Zhang, B. C., Liu, R. Y., Dunlop, M. W., Lockwood, M., Moen, J., et al. (2011). On the importance of interplanetary magnetic field |By| on polar cap patch formation. *Journal of Geophysical Research*, *116*(A5), A05308. https://doi.org/10.1029/2010JA016287